The Effect of Trace Impurities on the Stress-Corrosion Cracking Susceptibility and Fracture Toughness of 18 Ni (300 Grade) Maraging Steel

by

R. P. M. Procter* and H. W. Paxton

Metallurgy & Materials Science
Carnegie-Mellon University
Pittsburgh, Pennsylvania 15213

METALS RESEARCH LABORATORY
CARNEGIE INSTITUTE OF TECHNOLOGY

Carnegie-Mellon University

PITTSBURGH, PENNSYLVANIA

The Effect of Trace Impurities on the Stress-Corrosion Cracking Susceptibility and Fracture Toughness of 18 Ni (300 Grade) Maraging Steel

by

R. P. M. Procter* and H. W. Paxton

Metallurgy & Materials Science
Carnegie-Mellon University
Pittsburgh, Pennsylvania 15213

January 1970

(To be submitted in part for publication)

* Presently, Research Metallurgist, Olin Corporation, Metals Research Laboratories, New Haven, Connecticut

This research was supported by the Advanced Research Project Agency, Order #878, Department of Defense under Nonr-760(31).

Abstract

A series of 18 Ni (300 grade) maraging steels of overall commercial purity but containing also deliberate impurity additions of sulphur, phosphorus, carbon, chromium and silicon + manganese has been studied. The fracture toughness and stress-corrosion resistance (determined using plane-strain fatigue-precracked specimens tested in 3.5% sodium chloride solution) of these steels have been compared to the fracture toughness and stress-corrosion resistance of a commercial purity 18 Ni (300 grade) maraging steel with no deliberate impurity additions, and to a similar steel prepared from special high-purity melting stock. The most important conclusions reached are that: (i) Ultra-high purity steels do not have significantly improved stress-corrosion resistance but show useful increases in fracture toughness when the carbon content is less than 0.005%; (ii) Simultaneous additions of Mn + Si result in extremely low fracture toughness values; (iii) High carbon contents (greater than 0.03%) result in marginally improved stress-corrosion resistance; (iv) High Cr contents result in rather poor stress-corrosion properties. These results have been correlated with the electron transmission microstructure of the steels and the results of a fractographic analysis of the fracture surfaces.

I. Introduction

Although there is currently considerable controversy as to whether or not pure metals are susceptible to stress-corrosion cracking (1), there is general agreement that high-purity metals are very often more resistant to this phenomenon than those of commercial purity. Furthermore, very small traces of impurities (for example 0.004% P in Cu (2)) can result in large differences in stress-corrosion resistance. These observations obviously have many practical and theoretical implications. The objectives of the present work, therefore, were to determine the effect of the commercially present impurities on the stress-corrosion cracking susceptibility of 18 Ni (300 grade) maraging steels, in the hope that useful improvements in their stress-corrosion resistance might be obtained, and also that the effects of particular impurities might give some insight into the mechanism of environmentally-induced sub-critical crack growth in these steels. The 18 Ni maraging steels were chosen firstly, because their stress-corrosion properties are already superior to those of low-alloy martensitic steels of equal strength (3) and thus any further improvement would be of practical importance. Secondly, the advanced melting practices used in the production of maraging steels offer the best hope for the commercial production of special steels of relatively high purity and very closely controlled chemistry. It was also of interest to compare the effects of trace impurities on the fracture toughness of maraging steels with similar effects in low-alloy high-strength steels (4).

II. Materials and Experimental Procedures

1. Materials

The alloys investigated were based on the 18 Ni (300 grade) maraging steel, of nominal composition:

Ni	Co	Mo	Al	Ti	Fe
18	9	5	0.1	0.75	Balance

Seven steels were studied. Five were prepared from commercial-purity melting stock with deliberate (nominal) additions of 0.025% S, 0.025% P, 0.50% C, 0.30% Cr and 0.15% Si + 0.15% Mn respectively. The stress-corrosion cracking susceptibility and fracture toughness of these steels were then compared with two further steels which had been prepared without deliberate impurity additions, one from the same commercial-purity melting stock and the other from specially purchased high-purity elements.

Each steel was produced as a 30 lb. vacuum-induction melt (see Appendix I. A.) by the Paul D. Merica Research Laboratory of the International Nickel Company, whose assistance is gratefully acknowledged. This laboratory also provided some of the compositional analyses shown in Table 1; extension of these analyses to other elements was by independent spectrochemical analysis.

Compositional effects are discussed in greater detail later in light of the experimental results reported below, but two points may be noted here. Firstly, for all elements except carbon, the target compositions were approximately attained, with respect to both the actual concentration levels of each element and the absence of unintentional compositional variations between steels. With carbon, however, there were unexpectedly large variations in concentration between steels, which made interpretation of the experimental results more difficult. Secondly, the steel prepared from the nominally high-purity starting materials was only marginally purer than the steel prepared from commercial-purity melting-stock, in spite of the fact that the former steel was prepared from specially purchased elements which, according to the suppliers' claims, should have resulted in a steel of significantly greater purity. This unsatisfactory composition of the high-purity steel may probably be attributed to over-optimism on the part of the suppliers combined with pick-up of tramp elements during melting.

To facilitate interpretation of the stress-corrosion data it was considered essential that all the steels be studied at the same strength level. Preliminary experiments (see Appendix I. B.) indicated that the presence of specific impurity additions did not significantly affect the aging kinetics; a single aging curve very similar to others reported in the literature (5, 6) was obtained. All the steels were therefore austenitized for 1 hour at 1500°F (816°C) and aged for 6 hours at 900°F (482°C), as recommended commercially; no other heat treatment conditions were investigated.

The mechanical properties of the experimental alloys after heat-treating were determined using non-standard tensile specimens of the design shown in Figure 1(A). The results obtained are reported in Table 2 (see Appendix II. A for experimental details). The yield and tensile strengths were somewhat lower than it had been hoped would be achieved.

II. 2. Stress-Corrosion and Fracture Toughness Tests.

All the stress-corrosion testing undertaken involved the use of fatigue-precracked, plane-strain specimens loaded in a cantilever-beam configuration, as illustrated in Figure 1B. Fracture mechanics concepts were used to analyse the experimental data, after Brown (7) and Freed and Krafft (10) (see Appendix II. B.). The stress-corrosion specimens were machined to their final dimensions after austenitizing but before maraging. Fatigue precracking however, was carried out, according to the A.S.T.M. recommendations (8), after maraging; the precrack was of type RW. (9). The fracture toughness of the steels was determined on specimens basically similar in design and dimensions to those illustrated in Figure 1(B) with the exception that they were ground from the failed stress-corrosion specimens; their total length therefore, was 8 1/2 ins. with the notch and fatigue precrack located 3 1/2 ins. from one end.

All stress-corrosion testing was undertaken in an aerated 3.5% NaCl solution controlled at 40°C (see Appendix II. C.), this environment was prepared from reagent-grade sodium chloride and distilled water and was of pH 6.3-6.6. Sufficient material was available to prepare eight stress-corrosion specimens from each alloy. These were used conventionally to estimate $K_{Is.c.c.}$ for each steel. $K_{Is.c.c.}$ was always approached from both above and below (see Appendix II. D.). In each case, however, only one value of $K_{Is.c.c.}$ was observed, indicating insignificant crack-blunting by corrosion.

II. 3. Electrochemical Measurements and Metallography

As reported below, significant differences in fracture toughness and stress-corrosion susceptibility were observed between the steels. In an attempt to correlate these differences with variations in the electrochemical characteristics of the steels, polarization studies were undertaken. Anodic and cathodic polarization curves for all the steels were determined in the same environment used for the stress-corrosion studies; the apparatus used is shown diagrammatically in Figure 2 and has been described in detail elsewhere (11). Conventional experimental procedures were used to generate the polarization curves (see Appendix II. E.).

Attempts were also made to correlate the differences in stress-corrosion resistance and fracture toughness with microstructure. Optical metallography, electron transmission microscopy and electron fractography were used (see Appendix II. F.).

III. Experimental Results

1. Stress-Corrosion and Fracture Toughness Tests

The dry-air plane-strain fracture toughness values, K_{Ic}, determined for the seven steels are shown in Table 3. Statistical analysis indicated that there were no significant differences in the fracture toughness of steels B, D, E and F at the 90% confidence level; their mean value of K_{IC} was

56.5 ± 2.5 k.s.i.√i. Both steels A and C however, had a significantly higher fracture toughness, within the range 65-68 k.s.i.√i; from the compositions shown in Table 1 it is apparent that very low carbon contents have a beneficial effect on fracture toughness but that the deleterious effect of increasing C additions soon reaches a limiting value (at about 0.01%) and thereafter, within the range investigated, does not continue to increase. The fact that the sulphur-containing steel had a purity similar to that of the high-purity steel with respect to all elements except S and Ti indicates that the observed high K_{Ic} values must be due to the low C contents of both steels. The relatively high purity of the S-containing steel is attributed to the Fe-Ti wash-out melt (see Appendix 1.A). Finally, steel G, containing simultaneous additions of Si + Mn had a significantly lower fracture toughness (~45 k.s.i.√i); this can only be attributed to the presence of one or both of these impurity additions.

Also reported in Table 3 are K_{Ix} values (the apparent fracture toughness determined from the final fracture in the stress-corrosion tests or, in other words, the stress-intensity required for rapid crack propagation from a stress-corrosion crack as opposed to a fatigue crack) for the seven steels. These values together with the values of $S \equiv K_{Ix}/K_{Ic}$, in Carter's terminology(3) the index of crack blunting, are discussed below in conjunction with the stress-corrosion results.

Figure 3(A) is a macrograph of the fracture surface of a fracture toughness specimen; the flat fracture and absence of significant shear lips indicates that plane-strain conditions had been satisfactorily achieved. Figure 3(B) illustrates the appearance of a failed stress-corrosion specimen. (In both the preceding illustrations, region A is the machined starter notch, B the fatigue precrack, C the stress-corrosion crack and D the final rapid fracture surface). It should be noted that on the stress-corrosion specimens somewhat wider shear lips were observed and this, combined with a plastic hinge effect may account partially for some of the high K_{Ix} and S values observed.

On a macroscale, no significant amounts of crack branching were observed and in all cases a single stress-corrosion crack propagated from the initial fatigue-precrack through to the final failure. In particular, two widely divergent cracks, as noted by Carter (3), were never observed.

In all cases, the stress-corrosion cracks propagated intergranularly with respect to the prior-austenite grain-boundaries, as illustrated in Figure 4. This is in accordance with the observations of other authors (12, 13). The fatigue-precrack was always transgranular. The appearance and path of the stress-corrosion cracks seemed independent (within the limitations of optical metallography) of the presence or absence of any particular impurity.

Separate curves of K_{Ii}, the initial plane-strain stress intensity against log t_f, the time to failure in the stress-corrosion tests are shown for each of the seven steels investigated in Figure 5. In all cases, the original data points for both failure and no-failure tests are indicated; from these points, the illustrated curves of K_{Ii} against log t_f were constructed and the estimates of $K_{Is.c.c.}$ reported in Table 3 obtained. Figure 5 gives an indication of the good reproducibility that may be obtained by the use of fatigue-precracked stress-corrosion specimens. For purposes of comparison, Figure 6 shows the curves of K_{Ii} against log t_f for all seven steels replotted on one graph, with the experimental data points omitted for the sake of clarity. The data reported in Figures 5 and 6 indicate that specific impurity additions had the following effects on the stress-corrosion resistance of 18 Ni maraging steel:

(i) There were no significant differences in the $K_{Is.c.c.}$ values for steels A, B, C and G, a value of about 10 k.s.i.$\sqrt{i}$ being observed in each case. In other words, the use of ultra-high purity maraging steel will not result in significantly improved stress-corrosion resistance compared to steels of normal commercial purity. Furthermore, unusually high S contents (up to 0.03%) and Mn + Si additions (up to 0.15% of each) will will not have any deleterious effect on stress-corrosion resistance. Note that all these steels have roughly the same S-value (3) (in the range 1.5 - 1.6). If it is assumed that the value of S is in some way predominantly

dependent on the nature of the stress-corrosion crack tip this result is to be expected.

(ii) Steel F had a slightly lower stress-corrosion threshold ($K_{Is.c.c.}$ ~8 k.s.i.$\sqrt{i}$) and there is thus preliminary evidence that high Cr residuals in the 18 Ni maraging steel may be detrimental to optimum stress-corrosion resistance. Other authors (3) have observed that the 12 Ni-5Cr maraging steels usually have poor stress-corrosion resistance and there is thus considerable circumstantial evidence that high Cr levels in general are incompatible with good stress-corrosion resistance in maraging steels. It is significant that steel F, with the lowest $K_{Is.c.c.}$, had the highest S value.

(iii) Steels D and E had a significantly higher $K_{Is.c.c.}$ value (~13 k.s.i.$\sqrt{i}$); this is associated with the presence of high phosphorus and carbon contents respectively. Again, it is significant that these two steels had the same fracture toughness as the commercial purity steel but that the K_{Ix} values were very low, leading to low S values. There is however, some difficulty in interpreting this data solely in terms of alloy composition as steel D, in addition to containing a deliberately high phosphorus addition, also contained significantly more carbon than the other steels.

No consistant correlation of any sort between K_{Ic} and $K_{Is.c.c.}$ or between K_{Ic} and K_{Ix}, was apparent for the seven steels, within the relatively narrow variations in these parameters which were observed. There was however, a correlation between the ratio K_{Ix}/K_{Ic} and the value of $K_{Is.c.c.}$, high values of S being associated with low $K_{Is.c.c.}$ values, and vice versa. If as suggested above, the value of the ratio S is in some way dependent on the nature of the stress-corrosion crack tip, this correlation is to be expected.

The curves shown in Figure 6 indicate that at a particular K_{Ii} value, the steels show different failure times and, on a semiquantitative basis, they may be interpreted as indicating that the stress-corrosion crack growth rate at a particular stress-intensity K_I varies between steels. The situation is, however, not quite so simple. Three factors are involved:

Firstly, although the specimens were fatigue precracked and then loaded with environment present, there was nevertheless still a distinct initiation period before crack propagation commenced. This was clearly demonstrated by monitoring the deflection of the loading arm with time; this gives a qualitative estimate of the rate of crack growth (a quantitative estimate cannot be obtained due to net-section yielding and varying plastic zone size). Figure 7 shows curves of the loading arm deflection with time. Curve A shows the typical deflection observed during the initial stages of the test. After the application of the load and transient creep in the apparatus there was a stable stage when no crack growth was apparent; this is regarded as the initiation time T_i for stress-corrosion crack propagation from a fatigue-precrack. This initiation time was measured in this way on all the steels, at varying K_{Ii} values, and typically had a value of 5-15% of the total time to failure. This variation is regarded as random experimental error, as no systematic variation with either composition or K_{Ii} value was noted. During stress-corrosion crack propagation, especially during the latter stages of the test when the crack was propagating very rapidly, discontinuities were apparent in the deflection-time curve, (as shown in curve B in Figure 7); these are interpreted as evidence of discontinuous crack growth. The existence of an initiation period and of evidence for discontinuous crack propagation are considered to be most consistent with a hydrogen-embrittlement mechanism of crack growth.

Secondly, as the steels show different K_{Ix} values, the extent of stress-corrosion crack propagation required to increase K_I to K_{Ix}, and hence cause failure varies. However, data by Mostovoy et. al. (14), Peterson et. al (15) and Johnson and Paris (16) indicate that for steels, the rate of stress-corrosion crack growth increases rapidly with stress-intensity at high K_I levels. The same conclusion may be reached by a comparison of curves A and B in Figure 7. It is therefore very probable that the bulk of the measured time to failure for

tests started at low K_I values consists of crack propagation at low K_I values (<~40 k.s.i.$\sqrt{i}$) and that the time required for propagation from say K_I = 40 k.s.i.$\sqrt{i}$ to K_I = 90 k.s.i.$\sqrt{i}$ is relatively short. The fact that the curves in Figure 6 appear asymptotic to some finite time (~300-700 mins) and do not tend to zero time as $K_{Ii} \rightarrow K_{Ic}$ is due to the fact that $K_{Ix} \neq K_{Ic}$. Thus, if a specimen is loaded to a K_{Ii} just below K_{Ic}, a finite time is required for the stress-corrosion crack to initiate and propagate to a point where $K_I = K_{Ix}$.

Thirdly, although 2 steels may be loaded to the same K_{Ii} value, if they have different $K_{Is.c.c.}$ values, then $\Delta K_I \equiv K_{Ii} - K_{Is.c.c.}$ will be different for the two tests. It has been shown elsewhere (17) that, for 4340 steel, the time-to-failure varies linearly as $1/\Delta K_I$. This has been interpreted (17) as indicating (a) that $V \alpha K_I (K_I - K_{Is.c.c.})^2$, where V is the stress-corrosion crack growth rate and (b) that the constant of proportionality in the above relationship varies directly as the slope of the straight line relationship. Figure 8 shows t_f plotted against $100/\Delta K_I$ for the steels used in the present investigation; a linear relationship is again observed. The fact that these straight line relationships are observed indicates that the crack initiation time, and the time required for crack propagation at high stress-intensity levels, do indeed, as argued above, make fairly small contributions to the overall failure time. It is also concluded that the steels containing P and C additions (D and E respectively) do in fact have significantly slower S. C. C. growth rates (at a given K_I level) than the other 5 steels, which otherwise show no marked relative differences in growth rate (cf. Figure 8).

III. 2. Electrochemical Measurements

Figure 9 shows on one plot the anodic and cathodic polarization curves for four of the steels (B, C, D and F), determined as described in Section II. 3. above. For the sake of clarity, the polarization curves for the other three steels (A, E and G) have been omitted; however, in all cases these latter lay within the envelope described by the four curves shown in Figure 9. It is

considered that there were no significant differences in the polarization curves of any of the seven steels investigated and that the apparent differences shown in Figure 9 are due to random experimental error. In any case, however the apparent differences between the polarization curves did not correlate in any way with the observed differences in $K_{Is.c.c.}$ or stress-corrosion crack growth rate. It was therefore concluded that these latter differences cannot be ascribed to obvious differences in the electrochemistry of the steels, as characterized by their potentiostatic polarization curves.

3. Metallographic Studies

The optical microstructure of the high purity steel (A) is shown at two different magnifications in Figure 10; it is essentially the same as those reported by other authors (18, 19) for similar steels after corresponding austenitizing and maraging treatments. Clearly visible are prior-austenite grain-boundaries and martensite laths within the grains. Although, as would be expected, all the other six steels had basically similar microstructures, the following significant differences were noted:

(i) Steel C (sulphur addition) contained very fine, light-etching inclusions, which are presumed to be some sulphide, as illustrated in Figure 11(A). This steel was the only one which exhibited any degree of banding and it was obvious that the sulphide particles were most prevalent in the bands; the banding itself, however, was not particularly marked (20).

(ii) Steel E (carbon addition) also contained a number of fairly fine inclusions, as illustrated in Figure 11(B); these particles, which were evenly distributed and not concentrated in grain-boundaries are assumed to be titanium carbonitride (20).

Apart from the above two steels, all the others had microstructures indistinguishable from that of the high-purity alloy (steel A), and none showed any signs of delamination during either the fracture toughness or the stress-corrosion tests; this might have been expected if serious banding existed.

The thin-foil transmission electron microstructure of the high-purity alloy (steel A) is shown in Figure 12. Again, this microstructure is essentially similar to that observed by other workers, who have identified the precipitates present, after a very similar heat treatment, as being orthorhombic Ni_3Mo and a complex tetragonal sigma phase probably based on FeTi (18). Boundaries are also visible, but it is not clear whether these are prior-austenite grain-boundaries, sub-grain boundaries or martensite lath boundaries; there is, however, some evidence of preferential precipitation on them. The other steels showed all of the above microstructural features but in addition, the Si + Mn containing alloy (steel G) showed a copious, evenly distributed dispersion of fairly coarse, rounded particles, as illustrated in Figure 13(A). The P- and C- containing alloys (steels D and E respectively) also contained a number of dispersoid particles, but these were fewer and less evenly distributed, as illustrated in Figures 13(B) and (C) respectively. No attempts were made at identification of the dispersoids in the Si + Mn or P alloys.

No fractographic examination of the fatigue-precrack fracture faces was undertaken. However, a detailed fractographic study of the rapid fracture surfaces of fracture toughness specimens was made and resulted in definite correlations between fracture toughness, alloy microstructure and the fracture surface morphology. In all the steels, the rapid fracture surface showed a transgranular, dimpled fracture morphology characteristic of ductile, overload failure by a mechanism of nucleation, growth and coalescence of microvoids (22,23). However, the Si + Mn steel, which had a low fracture toughness and which contained numerous, fairly coarse particles in addition to the strengthening precipitates (cf Figure 13(a) and comments above) showed a relatively uniform distribution of fine dimples, as illustrated in Figure 14(A). Higher magnification examination of these dimples indicated that they were usually nucleated by discrete particles, as illustrated in Figure 14(B); these particles are presumably the dispersoid discussed earlier. On the other hand, the steels with the highest fracture toughness

(the high-purity and sulphur containing steels, alloys A and C respectively) had a clean, dispersoid-free microstructure and generally showed a much coarser, though somewhat less uniform dimple size, as illustrated in Figure 15(A). Higher magnification examination of these dimples revealed some particles on the fracture surface but, as illustrated in Figure 15(B), these particles appeared to have nucleated microvoids only to a quite limited extent. Finally, although the four remaining steels (i.e. those with the constant, intermediate fracture toughness of about 56.5 k.s.i., alloys B, D, E and F) exhibited fairly wide variations in dimple size, as illustrated in Figure 16, the average dimple diameter was clearly intermediate between the fine and coarse dimples illustrated in Figures 14(A) and 15(A) respectively.

High magnification examination of the occasional very large dimples which were observed in the P- and C- containing alloys (steels D and E respectively) indicated that they had often been nucleated by brittle fracture of a large dispersoid particle, as illustrated in Figure 17(A). Occasionally the dispersoid particle itself was broken up by further plastic deformation of the matrix during subsequent growth of the microvoid, as illustrated in Figure 17(B).

Fractographic examination indicated that the stress-corrosion fracture surface morphology was essentially the same for all steels; no important or significant differences between alloys could be detected. In all cases, the fracture was brittle (in the sense of the absence of any evidence of gross or local plastic deformation as afforded by fatigue striations or dimples), intergranular with respect to the prior-austenite grain-boundaries, and in general quite similar to the stress-corrosion fracture surfaces observed in other high strength steels (17). The typical fracture morphology is illustrated in Figures 18(A) and (B). In some cases the fracture surfaces was quite heavily pitted (Figure 18(A)) while in others there seemed to be very little evidence of any chemical attack or corrosion. Both types of surface were, however,

observed in all steels and, in many cases, on adjacent areas of the same replica. In addition to pits, secondary cracks (X in Figure 18(B)) and grain-boundary surface markings (Y in Figure 18(B)) were also visible. These latter may be interpreted as evidence of residual ductility in a quasi-cleavage fracture mechanism.

IV. Conclusions

A series of 18 Ni (300 grade) maraging steels of overall commercial purity but containing also deliberate impurity additions of S, P, C, Cr and Si + Mn has been studied at a constant strength level. The plane-strain fracture toughness and the stress-corrosion resistance of these steels, as determined by testing plane-strain fatigue-precracked specimens in 3.5% NaCl solution, were evaluated. Comparison of these with the same parameters for a specially-produced high-purity 18 Ni (300 grade) maraging steel and a similar steel of commercial purity allows the following conclusions to be drawn:

(1) Production of ultra-high purity 18 Ni (300 grade) maraging steel, or of steel containing less than 0.005%C, will result in useful increases in fracture toughness but no significant improvements of stress-corrosion resistance.

(2) Increasing the carbon content within the range 0.01 to 0.06% results in no further progressive deterioration in fracture toughness but, within the range 0.03 to 0.06%C, can result in marginal improvements in stress-corrosion resistance, as evidenced by higher $K_{Is.c.c.}$ values and lower crack growth rates.

(3) The effect of phosphorus additions has not been clearly defined; up to 0.030%P does not have a deleterious effect on fracture toughness and may result in a marginal improvement in stress-corrosion resistance similar to that described for C.

(4) Chromium (0.24%) has no effect on fracture toughness but is detrimental to stress-corrosion resistance and results in slightly lower $K_{Is.c.c.}$ values.

(5) Simultaneous additions of Si + Mn result in a drastic reduction of fracture toughness but have no effect on stress-corrosion resistance.

(6) Sulphur additions (up to 0.03%) have no effect on either the fracture toughness or the stress-corrosion resistance.

The base-line data for the above comparisons are the fracture toughness and stress-corrosion resistance of the 18 Ni (300 grade) maraging steel of commercial purity.

The observed variations in fracture toughness have been correlated qualitatively with variations in the microstructure and the fracture surface morphology of the steels. Alloys with low fracture toughness exhibited fine dimples which had been nucleated by dispersoid particles in the microstructure, while alloys with high fracture toughness exhibited clean microstructures and coarse dimples. No similar correlation existed however, for the observed variations in stress-corrosion resistance, although an overall (inverse) correlation between K_{Ix}/K_{Ic} and $K_{Is.c.c.}$ was noted; this may be explained on the basis of the assumption that both quantities are in some way dependent on the conditions at the stress-corrosion crack tip. The differences in stress-corrosion resistance could also not be ascribed to variations in the electrochemistry of the steels so far as this could be characterized by anodic and cathodic polarization curves. As with AISI 4340 steel, a linear relationship was shown to exist between the time to failure, t_f and $1/\Delta K_I$ where $\Delta K_I \equiv K_{Ii} - K_{Is.c.c.}$. The implications of this type of relationship have been discussed in detail elsewhere (17).

The overall, practical conclusion which may be drawn is that for optimum stress-corrosion resistance and fracture toughness 18 Ni maraging steels should be as low as possible in both carbon and chromium, with the level of other elements being of much less importance. The improvement of stress-corrosion resistance noted with high carbon contents is not considered practically useful. Any definite interpretation of the effect of specific elements on stress-corrosion resistance in fundamental terms must await further conclusive evidence as to the mechanism of environmentally-induced subcritical crack growth in high-strength steels. Very tentatively however, it may be suggested that if the cracking is due to hydrogen-embrittlement, as is becoming increasingly probable, then the deleterious effect of Cr additions may be due to Cr dissolution and hydrolysis at the crack tip area leading to enhanced hydrogen evolution. On the other hand, preferential segregation of hydrogen to titanium carbo-nitride particles would result in improved stress-corrosion resistance because of lowered pH.

Acknowledgements

This research was supported by the Advanced Research Projects Agency of the Department of Defense under Contract Nonr-760(31) (A. R. P. A. Order Number 878, Coupling Program on Stress-Corrosion Cracking). It is a pleasure to acknowledge the useful advice of and discussions with Drs. A. M. Guzman, W. M. Leo and A. J. Stavros. The experimental assistance of Messrs. T. Kinne and W. Poling is also gratefully acknowledged.

References

1. H. H. Uhlig and D. J. Duquette, Corrosion Science, 9, 557, 1969
2. D. Thompson and A. Tracy, Trans. A.I.M.E. (I.M.D.), 185, 100, 1949
3. C. S. Carter, "Crack-Extension in Several High-Strength Steels Loaded in 3.5% NaCl Solution," The Boeing Company Report D6-19770 of November 1967
4. E. A. Steigerwald and C. Vishnevsky, "Literature Survey on the Influence of Alloy Elements on the Fracture Toughness of High Strength Steels," Army Materials and Mechanics Research Center Report AMMRC, CR 67-13 (F) of February 1968 (AD-665432)
5. D. T. Peters and C. R. Cupp, Trans. Met. Soc. AIME, 236, 1966 1420
6. S. Floreen and R. F. Decker, A.S.M. Trans. Quart., 55, 1962, 518
7. B. F. Brown, Mat. Res. and Standards, 6, 1966, 129
8. W. F. Brown and J. E. Srawley, "Plane Strain Crack Toughness Testing of High-Strength Metallic Materials," A.S.T.M. STP 410, Dec. 1966
9. Second Report of the Special ASTM Committee on Fracture Testing of High Strength Metallic Materials, Mat. Res. and Standards, 1, 1961, 389
10. C. N. Freed and J. M. Krafft, J. of Materials, 1, 1966, 770
11. A. J. Stavros, Ph.D. Thesis, Carnegie-Mellon University, 1969
12. S. W. Dean and H. R. Copson, Corrosion, 21, 1965, 95
13. R. N. Parkins and E. G. Haney, Trans. Met. Soc. A.I.M.E., 242, 1968, 1943
14. S. Mostovoy, H. R. Smith, R. G. Lingwall and E. J. Ripling, "A Note on Stress-Corrosion Cracking Rates, to be published in Eng. Frac. Mech.
15. M. H. Peterson, B. F. Brown, R. L. Newbegin and R. E. Groover, Corrosion, 23, 1967, 142
16. H. H. Johnson and P. C. Paris, Eng. Frac. Mech., 1, 1968, 3

17. R. P. M. Procter and H. W. Paxton, A.S.M. Trans. Quart., 62, 1969, 989

18. W. F. Spitzig, J. M. Chilton and C. J. Barton, A.S.M. Trans. Quart., 61, 1968, 635

19. A. Goldberg, A.S.M. Trans. Quart., 62, 1969, 219

20. B. G. Reisdorf, A.S.M. Trans. Quart., 56, 1963, 183

21. P. H. Salmon-Cox, B. G. Reisdorf and G. E. Pellissier, Trans. Met. Soc. A.I.M.E., 239, 1967, 1809

22. J. Plateau, G. Henry and C. Crussard, Rev. Met., 54, 1957, 200

23. C. D. Beachem and R. M. N. Pelloux, "Electron Fractography - A Tool for the Study of Micromechanisms of Fracturing Processes," A.S.T.M., STP 381, 1964, page 210

Steel	A	B	C	D	E	F	G
Nominal Composition	High Purity	Commercial Purity	Sulphur Addition	Phosphorus Addition	Carbon Addition	Chromium Addition	Si + Mn Addition
Ni	18.1	18.0	18.0	18.1	18.2	18.2	18.1
Co	8.87	9.00	8.90	8.97	9.00	8.87	8.83
Mo	5.00	4.97	4.85	4.98	4.90	4.97	4.97
Ti	0.69	0.76	0.79	0.76	0.76	0.76	0.75
Al	0.11	0.12	0.11	0.12	0.12	0.11	0.11
B	< 0.001	< 0.001	< 0.001	< 0.001	< 0.001	< 0.001	< 0.001
Zn	< 0.01	< 0.01	< 0.01	< 0.01	< 0.01	< 0.01	< 0.01
N_2	0.007	0.007	0.002	0.006	0.001	0.005	0.001
S	0.003	0.005	0.031	0.014	0.004	0.004	0.004
P	0.007	0.008	0.002	0.030	0.006	0.008	0.002
C	0.005	0.019	0.005	0.027	0.062	0.016	0.015
Cr	0.011	0.012	0.010	0.014	0.010	0.24	0.015
Si	0.014	0.015	0.014	0.018	0.011	0.017	0.15
Mn	0.024	0.025	0.025	0.025	0.025	0.025	0.14

Table 1

Composition of experimental alloys, in weight percent, with iron-balance

Steel	Composition	0.2% Offset Yield Strength k.s.i.	Tensile Strength k.s.i.
A	High-purity	244	249
B	Commercial-purity	246	253
C	S - Additions	240	247
D	P - addition	243	248
E	C - addition	240	245
F	Cr - addition	248	254
G	Si + Mn - additions	241	248

Table 2

Mechanical properties of experimental alloys

Steel	Composition	K_{Ic} (a)	K_{Ix}	S (b)	K_{Iscc}
A	High-purity	66	101	1.5	10
B	Commercial-purity	59	91	1.6	10
C	S-addition	67	98	1.5	10
D	P-addition	56	54	1.0	13
E	C-addition	58	47	0.8	13
F	Cr-addition	55	94	1.7	8
G	Si + Mn-addition	45	70	1.6	11

Table 3

Fracture toughness and stress-corrosion threshold stress-intensities for experimental alloys.

(a) Stress-intensities expressed in k.s.i.$\sqrt{in}$

(b) $S \equiv K_{Ix}/K_{Ic}$ (dimensionless)

Figure Captions

1. Design and dimensions of the specimens used for mechanical property determinations (A) and in fracture toughness and stress-corrosion tests (B).

2. Diagram of apparatus used in determination of potentiostatic polarization curves.

3. (A). Macrograph of the fracture surface of a fracture toughness test specimen; commercial purity alloy, steel B, measured K_{Ic} = 57.0 k.s.i.$\sqrt{i}$, x 5 approx.

   (B). Macrograph of the fracture surface of a stress-corrosion test specimen; chromium-containing alloy, steel F; K_{Ii} = 27.9 k.s.i.$\sqrt{i}$, K_{Ix} = 100 k.s.i.$\sqrt{i}$, time to failure = 333 minutes, x 5 approx.

4. Light micrograph of an intergranular stress-corrosion crack; chromium-containing alloy, steel F, x 500.

5. Individual curves of K_{Ii} against log t_f for the seven experimental alloys, showing all original data points.

6. Curves of K_{Ii} against log t_f replotted on one set of common axes, with original data points omitted.

7. Experimentally observed curves of loading arm deflection with time. Curve A: Carbon-containing alloy, steel E, K_{Ii} = 15.6 k.s.i.$\sqrt{i}$, K_{Ix} = 50 k.s.i.$\sqrt{i}$, failure time = 1885 minutes, initiation time ~255 minutes. Curve B: High-purity alloy, steel A, K_{Ii} = 15.3 k.s.i.$\sqrt{i}$, K_{Ix} = 107 k.s.i.$\sqrt{i}$, failure time = 1439 minutes.

8. Plots of t_f against $100/\Delta K_I$, showing linear relationship for all steels.

9. Selected anodic and cathodic potentiostatic polarization curves.

10. (A). Light micrograph showing typical microstructure of the high purity alloy, steel A, at x 200 magnification.

    (B). Light micrograph showing typical microstructure of the high purity alloy, steel A, at x 500 magnification.

11. (A). Light micrograph showing light-etching inclusions (arrowed) in sulphur-containing alloy, steel C, x 200.

    (B). Light micrograph showing dark-etching inclusions (arrowed) in carbon-containing alloy, steel E, x 200.

12. Thin foil electron transmission micrograph showing typical maraged microstructure of the high-purity alloy, steel A, x 61,000.

13. (A). Thin foil electron transmission micrograph showing coarse dispersoid particles in the microstructure of the Si + Mn containing alloy, steel G, x 27,000.

    (B). Thin foil electron transmission micrograph showing dispersoid particles in the microstructure of the phosphorus-containing alloy, steel D, x 25,000.

    (C). Thin foil electron transmission micrograph showing microstructure of the carbon-containing alloy, steel E, x 49,000.

14. (A). Electron fractograph of the rapid fracture surface of a fracture toughness specimen of the Si + Mn containing alloy, steel G, showing the fine dimpled morphology, x 2800.

    (B). As 19 (A), but at a higher magnification, showing nucleation of dimples (microvoids) by coarse dispersoid particles, x 12,000.

15. (A). Electron fractograph showing the coarse dimpled morphology of the rapid fracture areas of a fracture toughness specimen of the sulphur-containing alloy, steel C, x 1900.

    (B). Electron fractograph showing the coarse dimpled morphology of the rapid fracture area of a fracture toughness specimen of the high-purity alloy, steel A, x 8,000.

16. Electron fractograph showing mixture of coarse and fine dimples on the rapid fracture area of a fracture toughness specimen of the phosphorus-containing alloy, steel D, x 2800.

17. (A). Coarse dimple nucleated by brittle (cleavage) fracture of a titanium carbonitride particle on the rapid fracture surface of a fracture toughness specimen of the carbon-containing alloy, steel E, x 8,000.

    (B). Coarse titanium carbonitride particle fractured by plastic deformation of underlying metal; electron fractograph of the rapid fracture of a fracture toughness specimen of the carbon-containing alloy, steel E, x 12,000.

18. (A). Electron fractograph of the stress-corrosion fracture surface of the high purity alloy, steel A, showing pitting attack; x 2800.

(B). Electron fractograph of the stress-corrosion fracture surface of the commercial purity alloy, steel B, showing no pitting but secondary cracks (X) and grain surface markings (Y); x 2800.

BLANK PAGE

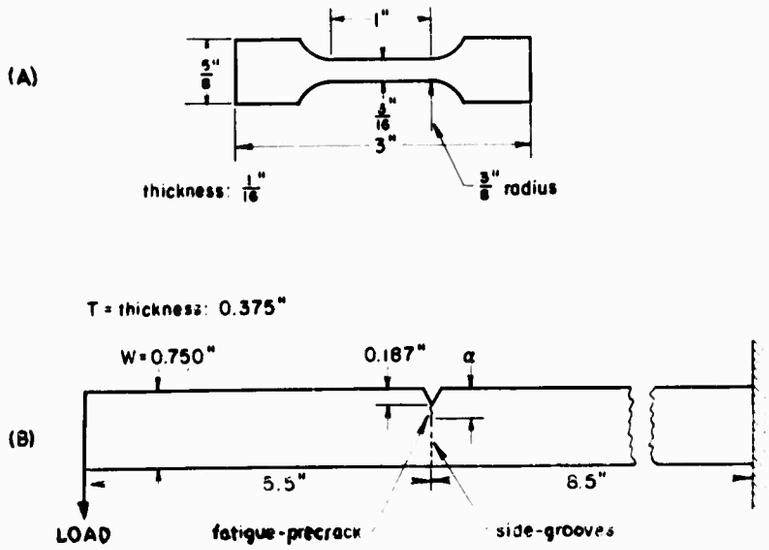

FIGURE 1

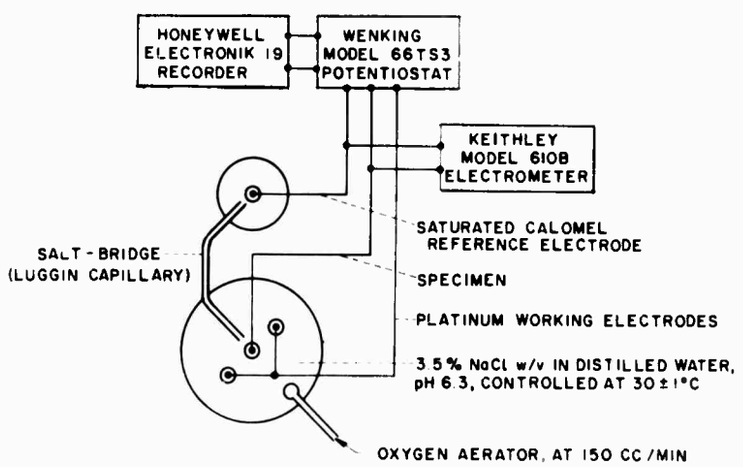

FIGURE 2

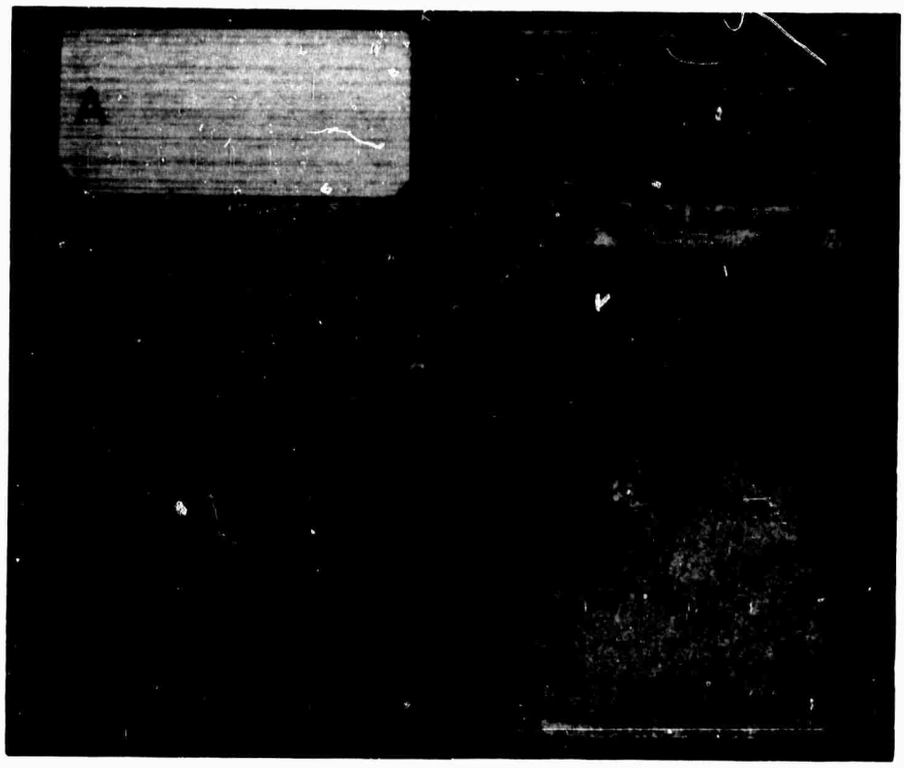

FIGURE 3 (A)

FIGURE 3 (B)

FIGURE 4

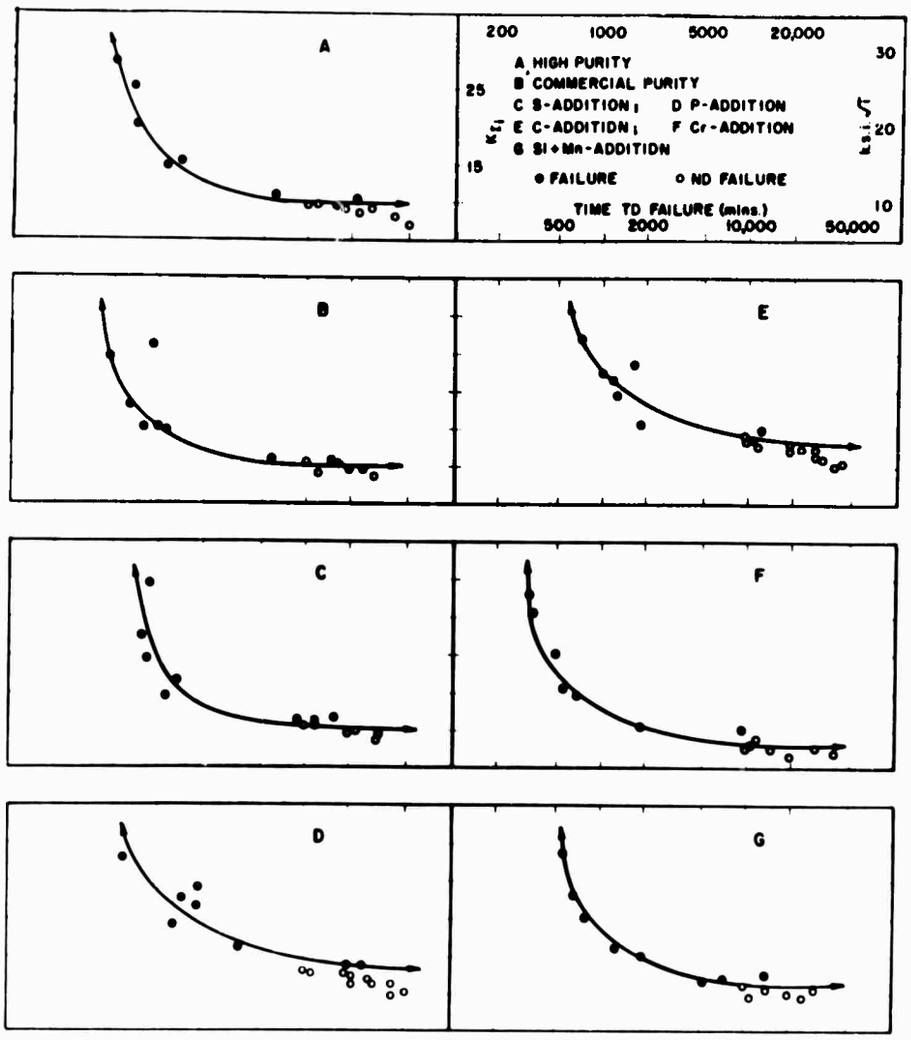
A
200
1000
5000
20,000
A HIGH PURITY
B COMMERCIAL PURITY
C S-ADDITION; D P-ADDITION
E C-ADDITION; F Cr-ADDITION
G Si+Mn-ADDITION
● FAILURE
○ NO FAILURE
TIME TO FAILURE (mins.)
500
2000
10,000
50,000
25
15
30
20
10
ksi
ksi √r
B
E
C
F
D
G

FIGURE 5

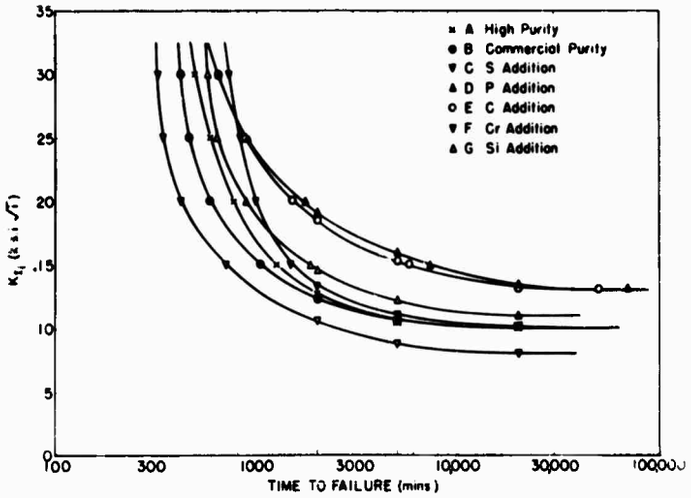
× A High Purity
● B Commercial Purity
▼ C S Addition
▲ D P Addition
○ E C Addition
▼ F Cr Addition
▲ G Si Addition
35
30
25
20
15
10
5
0
100
300
1000
3000
10,000
30,000
100,000
TIME TO FAILURE (mins)

FIGURE 6

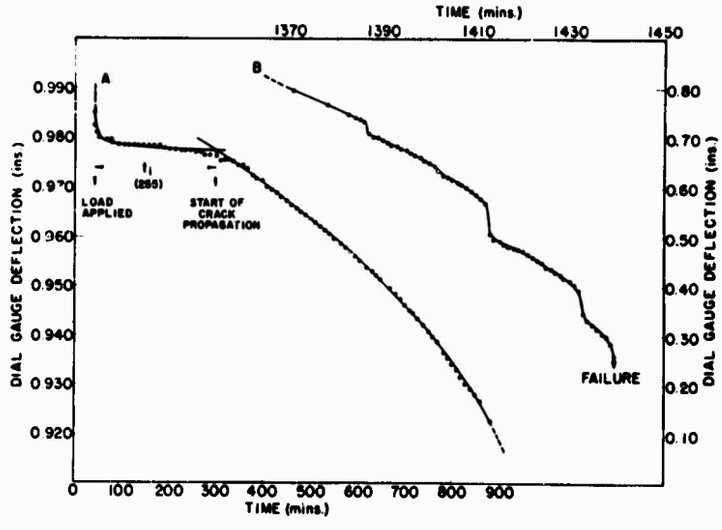

FIGURE 7

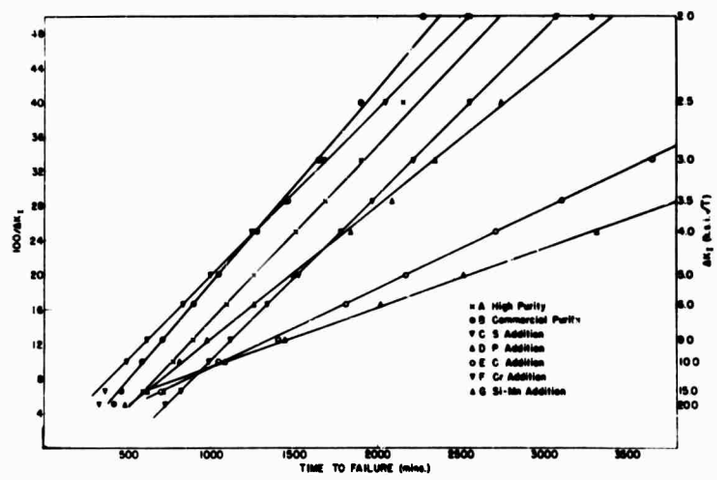

FIGURE 8

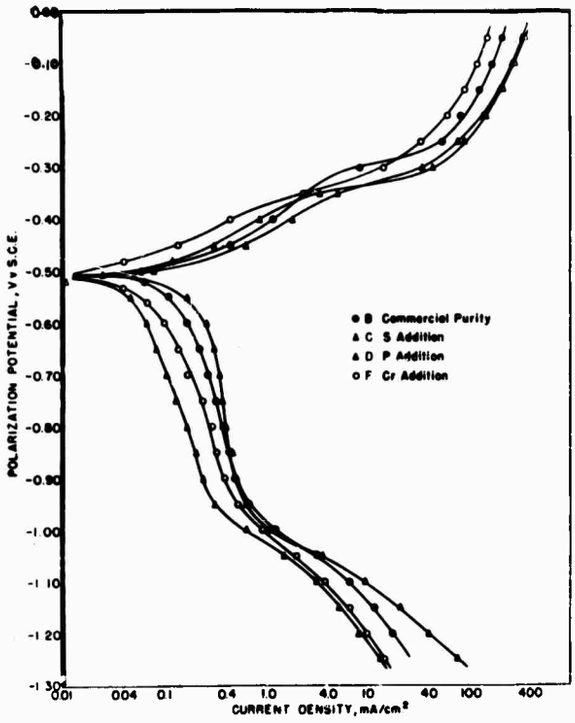

FIGURE 9

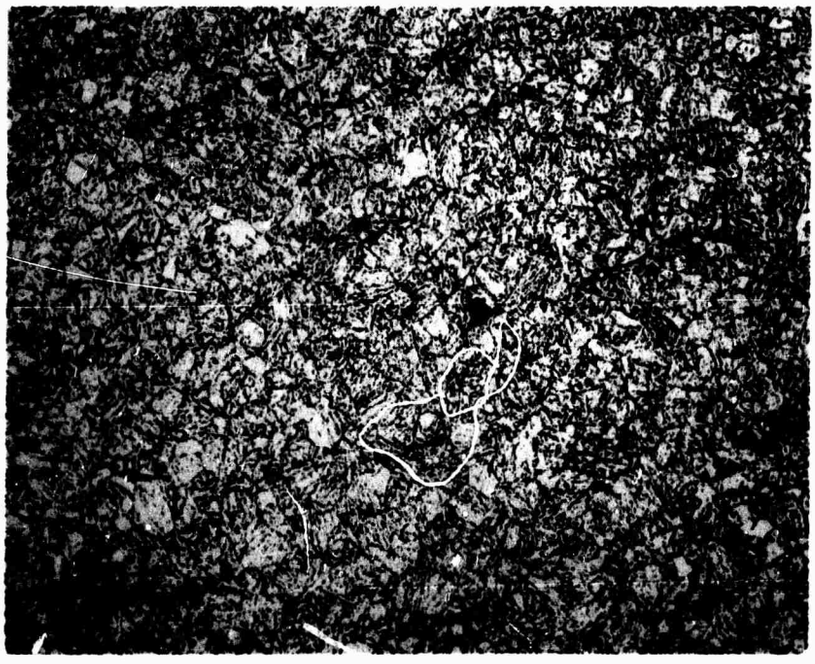

FIGURE 10 (A)

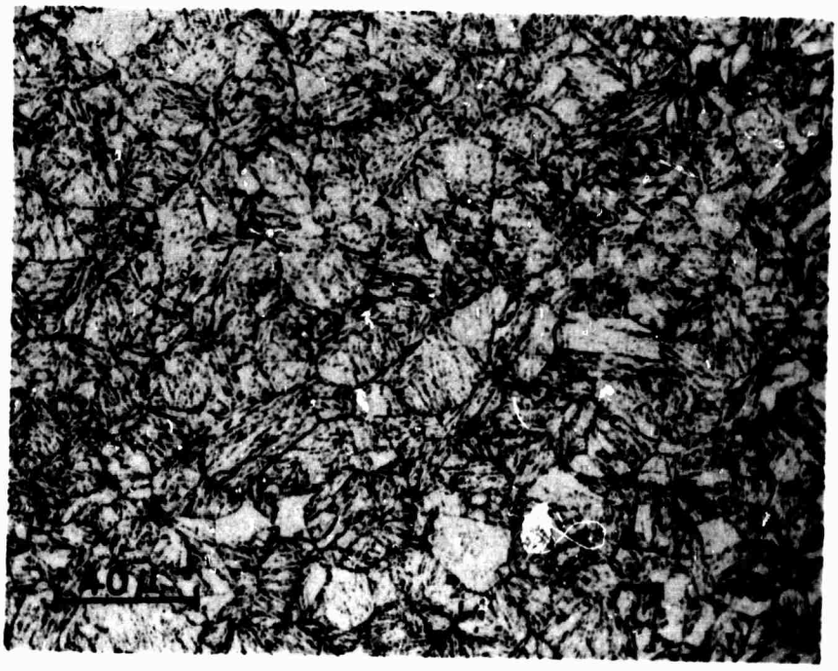

FIGURE 10 (B)

FIGURE 11 (A)

FIGURE 11 (B)

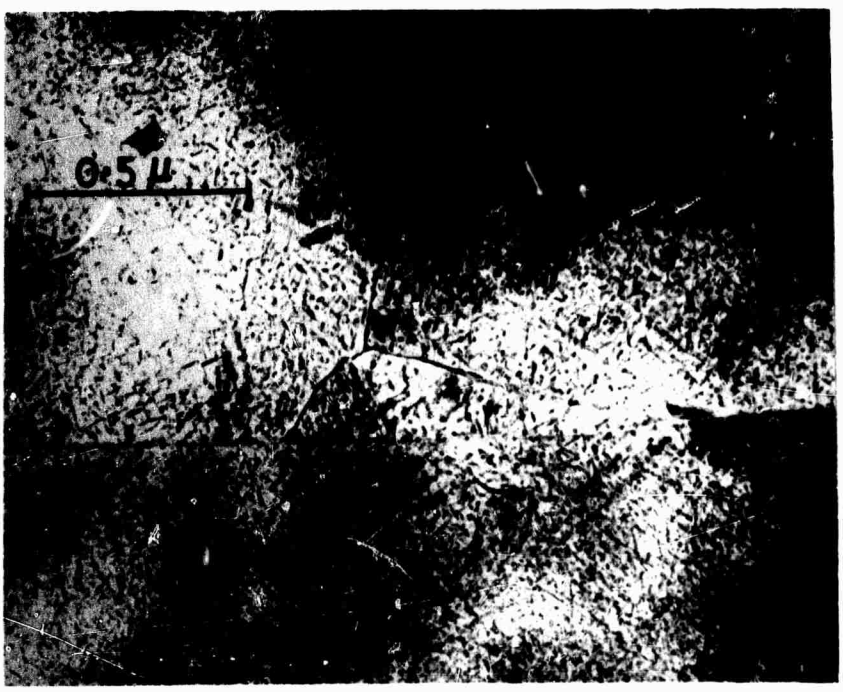

FIGURE 12

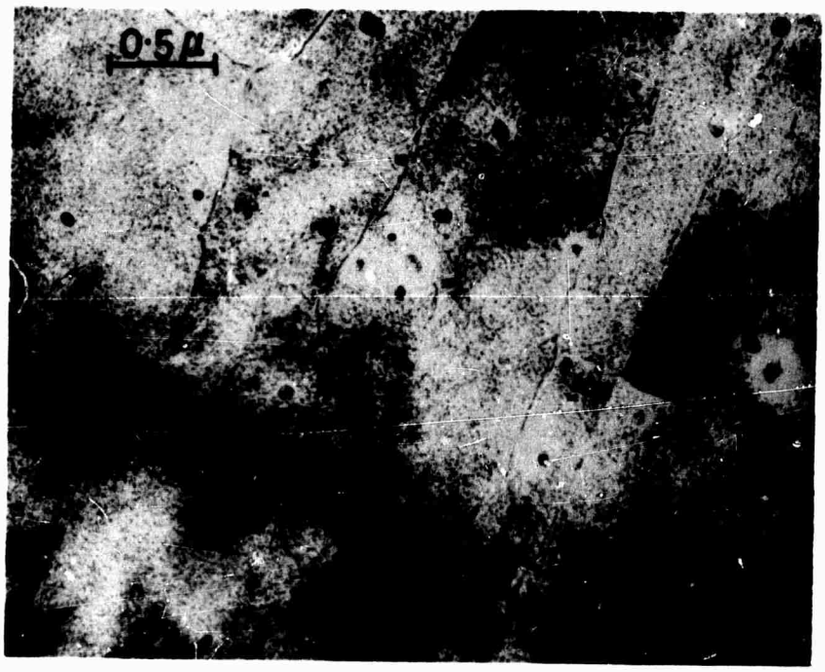

FIGURE 13 (A)

FIGURE 13 (B)

FIGURE 13 (C)

FIGURE 14 (A)

FIGURE 14 (B)

FIGURE 15 (A)

FIGURE 15 (B)

FIGURE 16

FIGURE 17 (A)

FIGURE 17 (B)

FIGURE 18 (A)

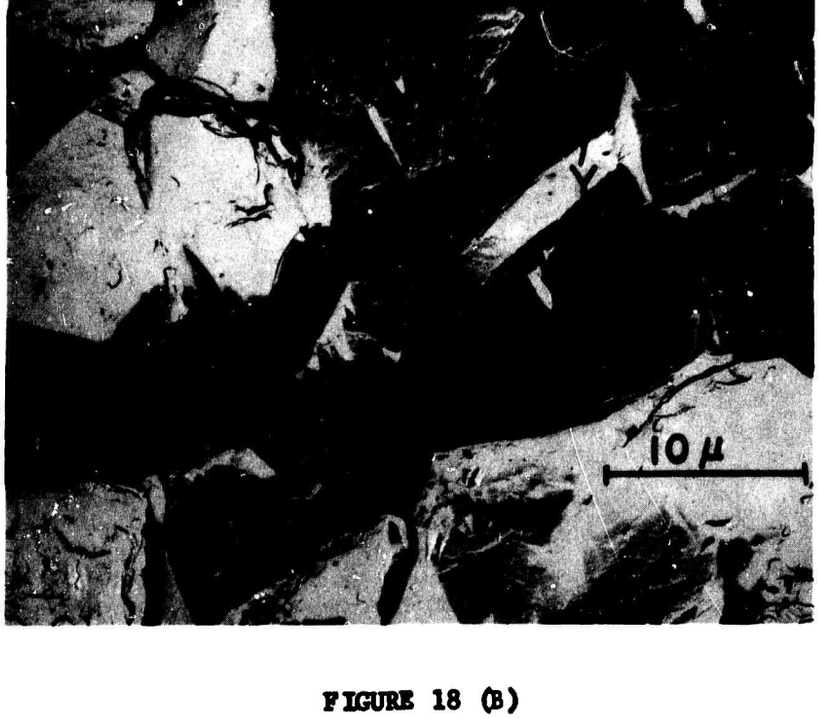

FIGURE 18 (B)

Appendix I - Preparation of Samples

A. The melting sequence used during preparation of the experimental alloys was: wash-out heat, commercial-purity heat, high-purity heat, C-addition heat, Cr-addition heat, Si + Mn addition heat, P-addition heat; the crucible was then washed out with an Fe-Ti alloy and finally the S-addition heat was melted. This sequence was designed to minimize the contamination from heat to heat. After melting, the ingots were soaked for one hour at 2300°F, flattened twice, resoaked for a further half hour at the same temperature, forged to 1.25" x 2.75" plate, and hot-rolled at 1900°F to 0.5" x 3.5" bars. Subsequent heat-treatments, as detailed in the text, were undertaken in the author's laboratory.

B. For each steel aging curves of hardness (R_c) against time (0.5 - 48 hours) at temperature (875, 900 and 925°F) after austenitizing for one hour at 1500°F were determined, using small (approx. 1/2 in. square) specimens. Within experimental accuracy, significant differences between the aging curves for different steels could not be detected and it was concluded that the presence of the impurities did not significantly affect aging kinetics. The aging curves obtained were very similar to corresponding curves reported in the literature (5, 6). Prior to testing, all the steels were therefore given the commercially recommended heat treatment of austenitizing for one hour at 1500°F (816°C), followed by maraging for 6 hours at 900°F (482°C). These heat-treatments were carried out in a 500 lb. neutral salt-bath and a gas-fired inert atmosphere furnace respectively; after both treatments the specimens were oil quenched. All the steels had final hardness values within the range R_c 54-57.

BLANK PAGE

Appendix II - Experimental Techniques

A. The longitudinal 0.2% offset yield strength, the ultimate tensile strength and the percent elongation of the seven steels were determined using non-standard tensile specimens of the design shown in Figure 1(A). These specimens were ground from failed stress-corrosion specimens and were pulled at a cross-head speed of 0.020 in/min. on a 10,000 lb. Instron, using double-wedge-action grips. The results obtained are shown in Table 2; each value is the mean of 3 specimens tested. These results confirm the preliminary hardness measurements and indicate no significant difference in mechanical properties between the steels. All the steels showed elongations of 4-5%.

B. Both the stress-corrosion and the fracture-toughness specimen dimensions were sufficiently large to ensure valid plane-strain conditions (8) and the stress-intensity at the crack-tip was therefore calculated using the formula (7):

$$K_I = \frac{4.12m\,(\alpha^{-3}-\alpha^{3})^{1/2}}{TW^{3/2}}\ \text{k.s.i.}\sqrt{\text{i}}$$

where $\alpha \equiv 1-\frac{c}{w}$ and m = bending moment at crack in kip-ins
T = specimen thickness in ins.
W = specimen width in ins.
c = total depth of notch + crack in ins.

The specimens were side-grooved to a depth of 5% of the total thickness on each side; the calculated K_I values were corrected for the presence of the side-grooves by the method of Freed and Krafft (10). The starter notch and side grooves in both the stress-corrosion and the fracture toughness specimens were inserted with a 60°, nominal 0.010" root-radius, V-cutter.

C. Polyethylene containers enclosing the area of the notch and fatigue precrack, as illustrated by Brown (7), were sealed to the specimens using a silicone adhesive (Dow-Corning Silastic 892 RTV). After application, the adhesive was allowed to cure fully for at least 24 hours before starting the test. The environment was circulated through the containers at a rate of 80-100cc./min., from a 30 liter reservoir maintained at 40 ± 1°C and fully aerated. The solution in the reservoir was changed weekly; in the interim, it became somewhat discolored by rust but the bulk solution pH remained within the original range of 6.3-6.6. In all cases the environment was admitted to the containers and allowed to circulate for 30 minutes prior to application of the load to the specimens. It would appear probable that this loading sequence minimized any initiation time required prior to crack propagation, as the load application produces a plastic zone at the crack tip which ruptures any pre-existing oxide film and thus bare metal is exposed to the environment, at least at the start of the test. All times were measured from the moment of application of the load.

D. For each steel six specimens were loaded to various initial stress-intensity levels, K_{Ii}, ($K_{Iscc} < K_{Ii} < K_{Ic}$) to generate curves of time-to-failure against K_{Ii} and hence to obtain from above an estimate of K_{Iscc}, the stress-intensity threshold below which stress-corrosion crack propagation does not occur. The other specimens were loaded to an initial stress-intensity of $K_{Ii} < K_{Iscc}$. After at least 10,000 minutes, if failure had not occurred and if no crack growth had taken place, (as measured by the deflection of a dial-gauge at the end of the cantilever loading-arm), the load was increased by a small increment; this procedure approached K_{Iscc} from below and was repeated until crack growth and failure resulted, i.e. until $K_{Ii} \geq K_{Iscc}$. Both methods gave the same estimate of K_{Iscc}, indicating that severe crack blunting by corrosion did not occur when $K_I < K_{Iscc}$. Three of the failed stress-corrosion specimens were used to make the fracture-toughness specimens

described in the text; K_{Ic} was estimated by increasing the load on the specimens until fracture occurred and then calculating the stress-intensity from the length of the initial fatigue-precrack and the load at fracture.

E. During determination of polarization curves the environment was maintained at 30±1°C and aerated by bubbling purified oxygen at a flow rate of 150 cc./min. Cylindical specimens, with a total exposed surface area of ~2.95 cm^2 were used; prior to testing these were abraded with 320 grade emery paper and then ultrasonically cleaned in acetone. These working-electrodes were machined from material from failed stress-corrosion specimens which had been reaustenitized at 1500°F for 1 hour; following machining the specimens were re-aged at 900°F for 6 hours. Two platinum counter-electrodes of similar design and dimension were used; these were cleaned by immersion for one minute in aqua regia immediately before use. All potentials were measured and are expressed with reference to a S. C. E. (add 242. 0mV to convert to S. H. E.). The initial potential of the specimens on immersion lay within the range -300 to -400 mV but was not reproducible and drifted considerably with time; after 20-25 hours, however, a stable, reproducible rest potential within the range -500 to -520 mV was obtained with all the steels. Starting from this rest potential, the cathodic polarization curve was determined first. The potential was stepped in the more negative direction in 50 mV increments, held potentio-statically, and, in each case, the cathodic current after 2 minutes recorded. This procedure was repeated until gas evolution occurred at the working electrode (at ~-1200 mV). At this stage, the external polarization was removed and within 2-3 hours the potential of the working electrode re-turned to, and remained stable at, the original rest potential. Using the same procedure, the anodic polarization curve was then determined. The sweep was continued until very severe dissolution was occurring at the working electrode (at ~0 mV); no passivation phenomena were observed.

F. Using optical metallography, specimens polished and etched in a solution containing 90 cc. ethanol + 5 cc. nitric acid + 5 cc. acetic acid were examined. To prepare foils for transmission electron microscopy, transverse specimens approx. 0.004 in. thick were ground from failed stress-corrosion specimens and then thinned to foils by jet-polishing in a 90% acetic acid - 10% perchloric acid mixture. To prepare specimens for electron fractography, a two-stage replication technique was used. An acetate replica of the original fracture surface was platinum shadowed (in growth direction at an angle of 30°) and then carbon deposited; finally the plastic backing was dissolved off in acetone in the usual way. Immediately after stress-corrosion or fracture toughness testing, but prior to replication, the fracture surfaces were always protected with an acetone-soluble lacquer.

Unclassified

Security Classification

DOCUMENT CONTROL DATA - R&D

(Security classification of title, body of abstract and indexing annotation must be entered when the overall report is classified)

1. ORIGINATING ACTIVITY (Corporate author)
Dept. of Metallurgy and Materials Science
Carnegie-Mellon University
Pittsburgh, Pa. 15213

2a. REPORT SECURITY CLASSIFICATION
Unclassified

2b. GROUP

3. REPORT TITLE
The Effect of Trace Impurities on the Stress-Corrosion Cracking Susceptibility and Fracture Toughness of 18 Ni (300 grade) Maraging Steel

4. DESCRIPTIVE NOTES (Type of report and inclusive dates)
Final Technical Report

5. AUTHOR(S) (Last name, first name, initial)
R. P. M. Procter and H. W. Paxton

6. REPORT DATE	7a. TOTAL NO. OF PAGES	7b. NO. OF REFS
January 1970	43	23

8a. CONTRACT OR GRANT NO.	9a. ORIGINATOR'S REPORT NUMBER(S)
Nonr-760(31) b. PROJECT NO. C-2 c. d.	9b. OTHER REPORT NO(S) (Any other numbers that may be assigned this report)

10. AVAILABILITY/LIMITATION NOTICES
Distribution of this document is unlimited and reproduction in whole or in part is permitted for any purpose of the U. S. Government.

11. SUPPLEMENTARY NOTES	12. SPONSORING MILITARY ACTIVITY
	Advanced Research Projects Agency Washington, D. C.

13. ABSTRACT

A series of 18 Ni (300 grade) maraging steels of overall commercial purity but containing also deliberate impurity additions of sulphur, phosphorus, carbon, chromium and silicon + manganese ~~had been~~ studied. The fracture toughness and stress-corrosion resistance (determined using plane-strain fatigue-precracked specimens tested in 3.5% sodium chloride solution) of these steels ~~have been~~ compared to the fracture toughness and stress-corrosion resistance of a commercial purity 18 Ni (300 grade) maraging steel with no deliberate impurity additions, and to a similar steel prepared from special high-purity melting stock. The most important conclusions reached are that: (i) Ultra-high purity steels do not have significantly improved stress-corrosion resistance, but show useful increases in fracture toughness when the carbon content is less than 0.005%; (ii) Simultaneous additions of Mn + Si result in extremely low fracture toughness values; (iii) High carbon contents (greater than 0.03%) result in marginally improved stress-corrosion resistance; (iv) High Cr contents result in rather poor stress-corrosion properties. These results ~~have been~~ correlated with the electron transmission microstructure of the steels and the results of a fractographic analysis of the fracture surfaces.

DD FORM 1 JAN 64 1473

Unclassified

Security Classification

Security Classification

14. KEY WORDS	LINK A		LINK B		LINK C	
	ROLE	WT	ROLE	WT	ROLE	WT
Maraging Steel						
Stress-Corrosion						
Impurities						
Fracture Toughness						
Fractography						

INSTRUCTIONS

1. ORIGINATING ACTIVITY: Enter the name and address of the contractor, subcontractor, grantee, Department of Defense activity or other organization *(corporate author)* issuing the report.

2a. REPORT SECURITY CLASSIFICATION: Enter the overall security classification of the report. Indicate whether "Restricted Data" is included. Marking is to be in accordance with appropriate security regulations.

2b. GROUP: Automatic downgrading is specified in DoD Directive 5200.10 and Armed Forces Industrial Manual. Enter the group number. Also, when applicable, show that optional markings have been used for Group 3 and Group 4 as authorized.

3. REPORT TITLE: Enter the complete report title in all capital letters. Titles in all cases should be unclassified. If a meaningful title cannot be selected without classification, show title classification in all capitals in parenthesis immediately following the title.

4. DESCRIPTIVE NOTES: If appropriate, enter the type of report, e.g., interim, progress, summary, annual, or final. Give the inclusive dates when a specific reporting period is covered.

5. AUTHOR(S): Enter the name(s) of author(s) as shown on or in the report. Enter last name, first name, middle initial. If military, show rank and branch of service. The name of the principal author is an absolute minimum requirement.

6. REPORT DATE: Enter the date of the report as day, month, year; or month, year. If more than one date appears on the report, use date of publication.

7a. TOTAL NUMBER OF PAGES: The total page count should follow normal pagination procedures, i.e., enter the number of pages containing information.

7b. NUMBER OF REFERENCES: Enter the total number of references cited in the report.

8a. CONTRACT OR GRANT NUMBER: If appropriate, enter the applicable number of the contract or grant under which the report was written.

8b, 8c, & 8d. PROJECT NUMBER: Enter the appropriate military department identification, such as project number, subproject number, system numbers, task number, etc.

9a. ORIGINATOR'S REPORT NUMBER(S): Enter the official report number by which the document will be identified and controlled by the originating activity. This number must be unique to this report.

9b. OTHER REPORT NUMBER(S): If the report has been assigned any other report numbers *(either by the originator or by the sponsor)*, also enter this number(s).

10. AVAILABILITY/LIMITATION NOTICES: Enter any limitations on further dissemination of the report, other than those imposed by security classification, using standard statements such as:

(1) "Qualified requesters may obtain copies of this report from DDC."

(2) "Foreign announcement and dissemination of this report by DDC is not authorized."

(3) "U. S. Government agencies may obtain copies of this report directly from DDC. Other qualified DDC users shall request through _____."

(4) "U. S. military agencies may obtain copies of this report directly from DDC. Other qualified users shall request through _____."

(5) "All distribution of this report is controlled. Qualified DDC users shall request through _____."

If the report has been furnished to the Office of Technical Services, Department of Commerce, for sale to the public, indicate this fact and enter the price, if known.

11. SUPPLEMENTARY NOTES: Use for additional explanatory notes.

12. SPONSORING MILITARY ACTIVITY: Enter the name of the departmental project office or laboratory sponsoring *(paying for)* the research and development. Include address.

13. ABSTRACT: Enter an abstract giving a brief and factual summary of the document indicative of the report, even though it may also appear elsewhere in the body of the technical report. If additional space is required, a continuation sheet shall be attached.

It is highly desirable that the abstract of classified reports be unclassified. Each paragraph of the abstract shall end with an indication of the military security classification of the information in the paragraph, represented as *(TS), (S), (C), or (U)*.

There is no limitation on the length of the abstract. However, the suggested length is from 150 to 225 words.

14. KEY WORDS: Key words are technically meaningful terms or short phrases that characterize a report and may be used as index entries for cataloging the report. Key words must be selected so that no security classification is required. Identifiers, such as equipment model designation, trade name, military project code name, geographic location, may be used as key words but will be followed by an indication of technical context. The assignment of links, roles, and weights is optional.

Unclassified

Security Classification